








Anthropogenic acidification of surface waters drives decreased biogenic calcification in the Mediterranean Sea

Sven Pallacks ^{1✉}, Patrizia Ziveri ^{1,2}, Ralf Schiebel³, Hubert Vonhof ³, James W. B. Rae ⁴,
Eloise Littley ^{1,4}, Jordi Garcia-Orellana ^{1,5}, Gerald Langer¹, Michael Grelaud ¹ & Belen Martrat⁶

Anthropogenic carbon dioxide emissions directly or indirectly drive ocean acidification, warming and enhanced stratification. The combined effects of these processes on marine planktic calcifiers at decadal to centennial timescales are poorly understood. Here, we analyze size normalized planktic foraminiferal shell weight, shell geochemistry, and supporting proxies from 3 sediment cores in the Mediterranean Sea spanning several centuries. Our results allow us to investigate the response of surface-dwelling planktic foraminifera to increases in atmospheric carbon dioxide. We find that increased anthropogenic carbon dioxide levels led to basin wide reductions in size normalized weights by modulating foraminiferal calcification. Carbon ($\delta^{13}\text{C}$) and boron ($\delta^{11}\text{B}$) isotopic compositions also indicate the increasing influence of fossil fuel derived carbon dioxide and decreasing pH, respectively. Alkenone concentrations and test accumulation rates indicate that warming and changes in biological productivity are insufficient to offset acidification effects. We suggest that further increases in atmospheric carbon dioxide will drive ongoing reductions in marine biogenic calcification in the Mediterranean Sea.

¹Institute of Environmental Science and Technology (ICTA), Autonomous University of Barcelona (UAB), Bellaterra, Barcelona, Spain. ²Catalan Institution for Research and Advanced Studies, Barcelona, Spain. ³Department of Climate Geochemistry, Max Planck Institute for Chemistry, Mainz, Germany. ⁴School of Earth & Environmental Sciences, University of St Andrews, St Andrews, UK. ⁵Department of Physics, Autonomous University of Barcelona, Bellaterra, Barcelona, Spain. ⁶Department of Environmental Chemistry, Spanish Council for Scientific Research (CSIC), Institute of Environmental Assessment and Water Research (IDAEA), Barcelona, Spain. ✉email: pallacks.s@gmail.com

Since the onset of the Industrial Revolution, human-induced climate change has rapidly modified the Earth system with notable impacts on the oceans. Rapidly increasing atmospheric carbon dioxide (CO_2) concentrations have resulted in global surface ocean pH decline of approximately 0.1 units compared to pre-Industrial levels¹, impacting the calcification process of marine calcifiers^{2,3}. Since the mid-19th century, enhanced CO_2 emissions have also contributed to global ocean surface warming by 0.76 ± 0.16 K between 1904 and 2016^{4,5}. In the second half of the 20th century, anthropogenically induced warming has also intensified vertical ocean stratification⁶, leading to changes in nutrient cycling and depletion of surface marine productivity⁷. These alterations of pH, temperature, and food availability are each assumed to influence the calcification rates of critical calcifying taxa such as planktic foraminifera^{8,9}, but their response to the combination of these factors is still unclear.

The Mediterranean is a primary climate change hot-spot that shows amplified climate responses to global change^{10,11}, making it a key region to investigate the response of marine ecosystems to human-induced changes of the chemical, physical, and biological environment. Due to its high alkalinity and the short residence times of its water bodies, the Mediterranean Sea is expected to have an exceptionally high uptake rate of anthropogenic carbon^{12–14}. Both annual mean surface air temperature and sea surface temperature (SST) have accelerated in the Mediterranean region compared to the global average since 1880 Common Era (CE)¹¹. The recent SST warming at a rate of 0.35 K per decade¹⁵, may result in thermally induced stratification and decreasing biological productivity¹⁶.

Comprehensive, multi-decadal monitoring of plankton communities started in 1931¹⁷, while time series measurements of seawater carbonate chemistry¹⁸ and surface ocean productivity¹⁹ began only in the late 20th century. As a result, observational time series are too short to reasonably attribute changes in the ocean's biological productivity to anthropogenically driven climate change²⁰. Laboratory experiments give important clues on how calcifying plankton copes with rapid climate change, but it remains difficult to capture the complex natural environment in a laboratory setting. Paleo-reconstructions of plankton calcification and accompanying records of environmental conditions can address these issues, providing records going back to pre-industrial times which could capture the impact of changing physical and chemical conditions on the marine ecosystem.

Here, we provide radiocarbon and radionuclide-dated, high-resolution marine proxy records from three locations in the western Mediterranean Sea (Fig. 1), covering the transition from the pre-industrial (pre-IE) to industrial era (IE), starting from about 1800 CE. With these we investigate the basin-wide, interspecies (*Globigerinoides elongatus* and *Globigerina bulloides*) response of planktic foraminiferal calcification (represented by the measured Size Normalized Weight, SNW) to warming, acidification, and variations in primary productivity, reconstructed using a suite of paleo proxies, over the onset of the Industrial Revolution. We show an unprecedented basin wide SNW decrease of 18% to 34% in the species *G. elongatus*, and 7% to 35% in *G. bulloides* over the 20th century. Enhanced uptake of anthropogenic CO_2 by Mediterranean surface waters as shown by decreasing planktic foraminiferal $\delta^{13}\text{C}$ (Suess Effect) and decreasing pH derived from boron isotopes ($\delta^{11}\text{B}$), brings us to the conclusion that anthropogenic CO_2 impairs foraminiferal calcification.

Results and discussion

Human induced sea surface warming and productivity changes in the western Mediterranean. The western Mediterranean Sea is a hotspot of rising SST, at a rate above the global average²¹, and

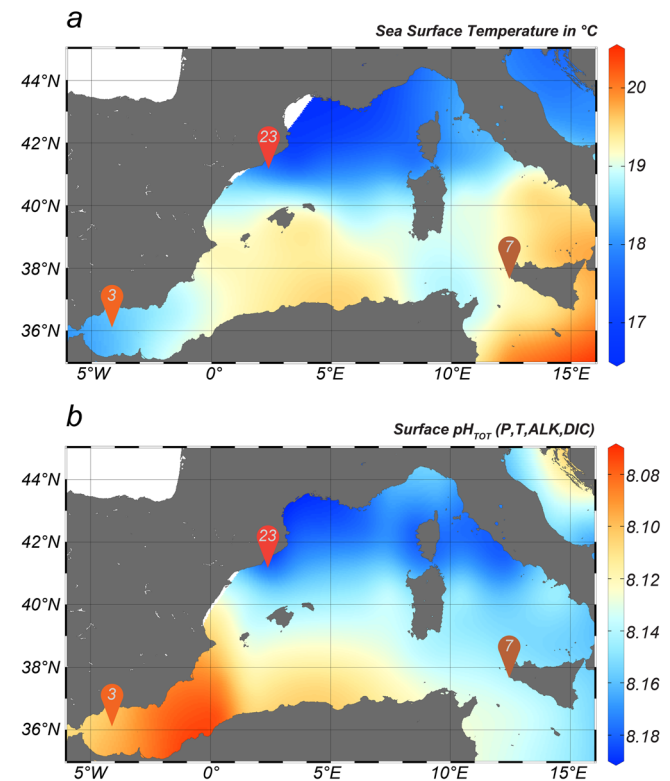


Fig. 1 Sea surface temperature (SST) and surface pH at the 3 study locations in the western Mediterranean basin. **a** Western Mediterranean SSTs from World Ocean Atlas 2018¹¹⁹. **b** Sea surface pH based on a global gridded dataset covering the period 1982–2020¹²⁰. Both maps are produced with Ocean Data View (version: 5.6.3)¹²¹. Red pins indicate core locations: MedSeA-S3-c1 (Alboran Sea; 3), MedSeA-S23-c1 (Balearic Sea; 23), MedSeA-S7-c2 (Strait of Sicily; 7).

anthropogenically-driven productivity changes during the IE¹⁶. Warming of western Mediterranean surface waters over the 20th century is shown by alkenone derived SST data and (HadISST) satellite time series observations (Figs. 2a, 3c). A mid-20th century cooling period by > 1 K in the Mediterranean from the end of the 1940s to the end of the 1980s is confirmed, as seen in other western Mediterranean paleotemperature records^{16,22}. This cooling episode is followed by rapid warming over the last 20 years. Any offsets between instrumental and paleorecords might be due to low data coverage for SST calibrations in the central Mediterranean (Supplementary Note 1). Indeed, while the Strait of Sicily alkenone record indicates warming just above average over the last two decades, other recently published paleorecords in the Alboran and Balearic Sea¹⁶ consistently show accelerated 20th century sea surface warming (Fig. 2a), with unprecedented warming rates at present in the Mediterranean Sea²³. High sea surface warming rates at our sites confirm a rapid, anthropogenically induced sea surface warming in the western Mediterranean.

Accelerated anthropogenic climate change has altered marine productivity in the Mediterranean Sea, as reflected by plankton community changes¹⁶. The sedimentation rate of planktic foraminiferal tests is positively related to primary productivity²⁴, while alkenone concentrations are closely related to phytoplankton biomass²⁵. Both foraminiferal tests and alkenones thus serve as proxies of changes in past ocean productivity and reflect surface productivity levels at all three study sites (Supplementary Note 1). In the Strait of Sicily, test accumulation rates decrease between the 1850s and 1940s, then increase rapidly, which, alongside increasing C_{37} alkenone concentrations, indicates

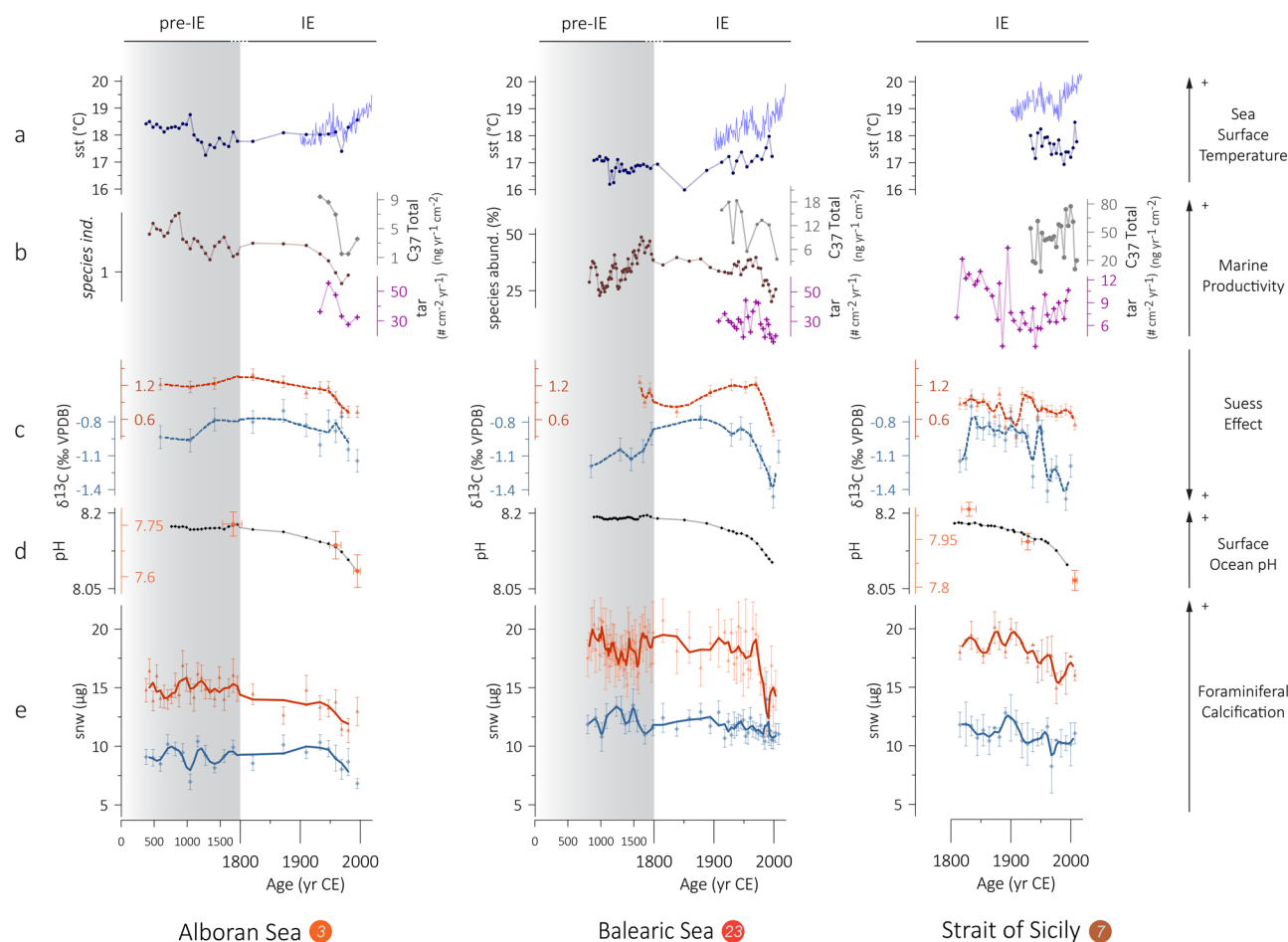


Fig. 2 Changes of sea surface conditions and planktic foraminiferal size normalized weight (SNW) over the Common Era at three western Mediterranean core sites (Alboran and Balearic Seas, and Strait of Sicily). **a** Sea surface temperature (SST) changes derived from alkenones (dark blue line) and the HadISST data set (light blue line). **b** Marine surface productivity represented by total test accumulation rate (purple line), alkenone concentration (grey symbols), and species composition (*G. bulloides* versus *G. inflata*) and species abundance (*G. inflata* + *G. truncatulinoides*) changes (brown line)^{16,122}. **c** Suess effect displayed through $\delta^{13}\text{C}$ (‰ VPDB) signature measured in planktic foraminiferal tests of *G. elongatus* (red dashed line) and *G. bulloides* (blue dashed line) with error bars indicating 0.1 ‰ uncertainty (1 SD level) and displayed as 3 point running average. **d** Surface ocean pH estimated with CO2SYS (black line- see methods) and boron isotope measurements (Orange symbols) in tests of *G. elongatus* (Alboran Sea) and *G. ruber albus* (Strait of Sicily), with vertical error bars indicating one standard deviation of uncertainty and horizontal error bars displaying age error range. **e** Planktic foraminiferal calcification expressed as SNW for *G. elongatus* (red) and *G. bulloides* (blue) with error bars indicating one standard deviation of uncertainty, displayed as 3 point running average. Grey shaded area in Alboran and Balearic time series represents the pre Industrial Era, prior to 1800 CE with a compressed time axis.

enhanced productivity during the second half of the 20th century (Fig. 2b). Biogeochemical model results²⁶ and historical records²⁷, confirm productivity increase in Mediterranean surface waters during the 20th century, and suggest enhanced anthropogenic nitrate and phosphate loads as the main driver of surface water eutrophication. In contrast, a decrease in productivity is observed in the Alboran and Balearic records during the second half of the 20th century (Fig. 2b). At these sites, enhanced stratification through 20th century SST increase likely explain surface productivity losses, which are also recorded through changes in planktic foraminiferal species composition¹⁶. Our results and previous studies thus show regionally distinctive patterns of 20th century productivity changes for the western Mediterranean.

Anthropogenic CO₂ intrusion into western Mediterranean waters recorded by planktic foraminiferal test chemistry. The $\delta^{13}\text{C}$ and $\delta^{11}\text{B}$ signatures of planktic foraminiferal tests provide sensitive tracers of anthropogenic carbon uptake and acidification

of the western Mediterranean Sea. While fluctuations in carbonate chemistry, productivity, and hydrography may modulate the carbon isotope signal, these influences are relatively small compared to the change in the isotopic composition of ambient seawater due to the input of low $\delta^{13}\text{C}$ CO₂ from fossil fuel burning (the Suess Effect)^{28–30}, making $\delta^{13}\text{C}$ a good tracer for natural versus anthropogenic environmental changes.

We use the two morphotypes of planktic foraminiferal species *Globigerinoides elongatus* (syn. *Globigerinoides ruber* white sensu lato) and *G. ruber albus* (syn. *G. ruber* white sensu stricto) as well as *Globigerina bulloides* to evaluate environmental alterations in the upper water column, as they are surface mixed layer dwellers³¹. As *G. bulloides* thrives in late winter/early spring and *G. ruber* in late spring/summer^{32,33}, we also cover most of the seasonal change in sea surface temperature and primary productivity.

At all three sites analyzed here, *G. elongatus* and *G. bulloides* show a notable $\delta^{13}\text{C}$ drop during the IE, against a backdrop of pre-industrial natural variability (Figs. 2c and 3d), which we refer to here as negative anthropogenic carbon isotope excursions

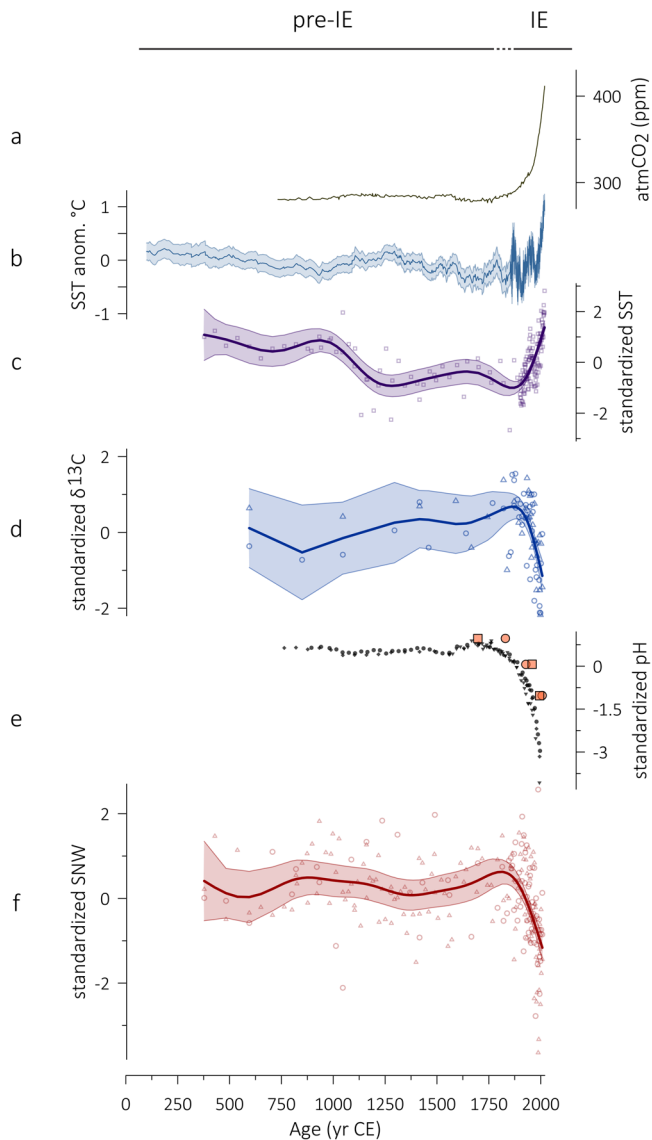


Fig. 3 Basin-wide changes of western Mediterranean sea surface conditions and planktic foraminiferal size normalized weight (SNW) over the Common Era driven by enhanced anthropogenic CO₂ emissions.

a Atmospheric CO₂ concentrations derived from measured¹⁰² and reconstructed^{103,104} records. **b** Stack of Mediterranean Sea Surface Temperature (SST) anomalies (blue line) with light blue shading indicating the 68% Confidence Interval²³. **c** Generalized additive model (GAM) fit (purple line) of standardized SST data (purple open squares) including alkenone derived SST¹²² and calculated mean from HadISST for each location. Purple shading indicates 95% Confidence Interval. **d** GAM fit (dark blue line) to standardized δ¹³C results comprising *G. elongatus* (blue triangles) and *G. bulloides* (blue circles) of all three stations, blue transparent ribbon indicates 95% confidence interval. **e** Standardized pH values (black symbols) estimated through CO₂SYS for Alboran Sea (diamonds), Balearic Sea (full circles) and Strait of Sicily (triangles). Standardized pH values derived from boron isotope measurements (orange symbols) in *G. ruber albus* at Strait of Sicily (circles), and in *G. elongatus* at the Alboran Sea (squares). **f** GAM fit (dark red line) to standardized SNW of *G. elongatus* (red triangles) and *G. bulloides* (red circles) of all three stations, red transparent ribbon indicating 95% confidence interval.

(nCIEs). nCIEs show most marked decreases during the latter half of the 20th century with a mean amplitude of -0.60‰ and range between -1.24‰ and -0.14‰ (Supplementary Fig. 1). We attribute these nCIEs to the increase of the surface ocean concentration of anthropogenic CO₂³⁴. The measured decline of δ¹³C in our foraminiferal tests during the second half of the 20th century describes a more pronounced Suess Effect signal when compared with results from the Northwest Atlantic (range = -0.174‰ to -0.757‰ ; weighted average = -0.45‰)³⁰.

Ocean uptake of anthropogenic CO₂ increases hydrogen ion (H⁺) concentrations and hence lowers pH³⁵. Boron isotope ratios of tests of *G. ruber albus* and *G. elongatus* reveal a notable pH decline in the Alboran Sea of -0.14 units between 1697 and 1995 CE, which is in accordance with previous estimates over the industrial period ranging from -0.06 to -0.16 units³⁶, and also notable ocean acidification in the Strait of Sicily, with reconstructed pH decreasing by 0.22 units from 1830 to 2007 CE. These results are largely consistent with the acidification expected from anthropogenic CO₂ invasion (Supplementary Fig. 2), which we calculate by assuming equilibrium between surface waters and the atmosphere alongside modern alkalinity and observed SST change at each site (see Methods); we note that absolute pH values from δ¹¹B are lower than recent pH levels (Fig. 2d) measured in the Mediterranean Sea^{37–41}, a feature that is discussed in more detail in the supplements (Supplementary Note 2). Slightly enhanced acidification in the Strait of Sicily might be caused by enhanced vertical mixing during the second half of the 20th century, transporting low-pH Mediterranean intermediate waters to the surface⁴² as indicated through enhanced productivity and SST cooling compared to other sites (Fig. 2a, b). Measurements reveal recent pH decreases between 0.0009 yr^{-1} and $0.0036\text{ pH units yr}^{-1}$ in the Alboran Sea⁴¹ and between 0.0013 yr^{-1} and $0.0030\text{ pH units yr}^{-1}$ in the North Western Mediterranean^{39,40}, which exceed the global average trend of $0.0017 \pm 0.0002\text{ pH units yr}^{-1}$ ⁴³. The rate of pre-industrial to modern pH decline is well-reflected by our boron isotope derived values and corroborated by CO₂SYS model estimates (Supplementary Fig. 2), suggesting acceleration of ocean acidification in western Mediterranean surface waters during the 20th century.

Whilst the nCIEs primarily reflect uptake of isotopically light CO₂ in the surface ocean, falling [CO₃²⁻] and pH levels tend to increase δ¹³C in foraminiferal tests⁴⁴, and could thus dampen the Suess Effect driven nCIE signal we observe. Based on laboratory and field data^{44–46}, western Mediterranean pH and [CO₃²⁻] changes since 1900 are estimated to account for approximately 0.24‰ to 0.33‰ (*G. ruber*) and 0.48‰ (*G. bulloides*) of δ¹³C test changes (Supplementary Table 1). Ambient water temperature changes have a minimal, negative effect on δ¹³C in foraminiferal tests^{45,47}, accounting for -0.12‰ in *G. bulloides* tests, when basing estimations upon SST warming rates in the western Mediterranean (Supplementary Table 1). Variability in upwelling strength and biological productivity can also influence δ¹³C in calcite tests at the species scale⁴⁵, as can algal or bacterial symbionts, which change the microenvironment of planktic foraminifera near the test surface impacting their δ¹³C signal^{48–50}. Strong pH and SST changes, differential upwelling, and productivity patterns at our three study sites are thought on the whole to slightly counter the Suess Effect and attenuate the full magnitude of the signal of decreasing δ¹³C in our planktic foraminiferal tests²⁹.

We conclude that the input of isotopically light anthropogenic CO₂ in the surface ocean has caused nCIEs during the IE in both *G. bulloides* and *G. elongatus* in the western Mediterranean Sea.

At the same time, enhanced CO_2 uptake by the ocean drives acidification, as indicated by boron isotope measurements and model estimates, attenuating the Suess Effect signal. Sea surface warming, upwelling, and changes in marine surface production during the 20th century have minor attenuating influences on the $\delta^{13}\text{C}$ signal.

Anthropogenic impacts on planktic foraminiferal calcification.

SNW is a useful tool for understanding the differential response of planktic foraminifera to climate change stressors like ocean warming, acidification, and productivity changes. SNW provides a normalized measure of chamber wall thickness and density, reflecting carbonate production and preservation of planktic foraminiferal tests⁴⁷, and is used as a proxy for past $[\text{CO}_3^{2-}]$ ^{9,51}, though has also been suggested to provide a potential proxy for growth rate in planktic and benthic foraminifera^{52,53}. Although secondary influences such as physico-chemical conditions of ambient seawater, and autecological properties can influence SNW, these do not seem to prevent the application of the proxy^{8,54}. We found that SNW of *G. elongatus* and *G. bulloides* decreased at all three stations throughout the last 200 yr., unprecedented against the backdrop of our ~1500 yr. long records in the Alboran and Balearic Seas (Figs. 2e; 3f). Basin-wide relative SNW loss during the 20th century in *G. elongatus* ranges from 18% to 34% and in *G. bulloides* from 7% to 35% (Supplementary Fig. 3).

Decreasing ocean pH and $[\text{CO}_3^{2-}]$ due to enhanced CO_2 uptake from the atmosphere can impede the biological precipitation of carbonate tests⁵⁵, depending on the species-specific response. Commonly, *G. elongatus* and *G. bulloides* reduce their test calcite mass with lower $[\text{CO}_3^{2-}]$, calcite saturation (Ω), and pH, shown by numerous studies based on sediment and water samples, sediment trap time series, as well as culture experiments^{9,51,56,57}. Despite this, in the natural environment, it is important to consider the combined influence of the various environmental drivers on planktic foraminiferal calcification, with studies using cultures, sediment traps, plankton nets and marine sediments attributing SNW changes to surface ocean carbonate chemistry, alongside temperature and productivity^{8,9,51,54,57–60}.

Sea surface warming decreases the solubility of atmospheric CO_2 , elevating $[\text{CO}_3^{2-}]$ in surface water, while higher temperature can also foster enzymatic activity, resulting in faster growth rates and enhanced calcification rates⁶¹. Both effects cause an increase in planktic foraminiferal SNW, a relationship observed in our target species in a number of earlier studies^{8,9,51,56,58,62}. Sea surface warming in the western Mediterranean, as shown in our records (Figs. 2a; 3c), should have enhanced SNW in both species over the IE if temperature were the leading influence. The negative correlation between SST and SNW of *G. elongatus* and *G. bulloides* at all three study sites during the IE, is indicative of an overriding effect of declining $[\text{CO}_3^{2-}]$ due to anthropogenic carbon input during the last 150 yr., masking any small opposing effect of temperature changes. Although temperature rise may have somewhat dampened the decrease in SNW, our results substantiate the dominant role of $[\text{CO}_3^{2-}]$ decline due to ocean acidification as the main driver of test calcite production.

Marine primary productivity in surface waters is assumed to influence test calcite production and therefore SNW^{8,63}. Test calcification is energy demanding⁶⁴, as greater food availability could allow foraminifera to allocate more energy to it. Chlorophyll *a* concentrations may serve as a proxy for marine primary productivity and food availability, as phytoplankton is considered to be the basis of planktic foraminiferal alimentation^{65,66}. However, the relationship between marine

primary productivity and SNW for our targeted species varies according to interspecific and intraspecific diversity and thus different calcification responses to changing trophic conditions. Previous studies detect weak positive/negative correlations between chlorophyll *a* and SNW for symbiont-bearing *G. bulloides*/symbiont bearing *G. elongatus* in the Atlantic Ocean^{8,58}, while a reverse correlation is observed for those species in the Mediterranean Sea⁶³. Evidence for a minor effect of varying productivity on the calcification response of planktic foraminifera is given by the fact that, despite opposing productivity signals during the second half of the 20th century (Fig. 2b), we see consistent SNW decreases in both species at all three stations (Figs. 2e; 3f).

Changes of the chemical test microenvironment due to photosynthetic activity also influences calcification of planktic foraminifera⁴⁸. Higher photosynthetic activity increases pH and reduces CO_2 concentrations near the shell, resulting in enhanced calcification rates⁴⁹. If enhanced stratification led to enhanced light availability during the 20th century, this would likely have increased SNW of planktic foraminiferal species associated with symbionts capable of performing photosynthesis, though this effect is evidently masked by the dominant role of $[\text{CO}_3^{2-}]$ on calcification. Diagenetic processes can bias the significance of SNW as a proxy for planktic foraminiferal calcification, as dissolution/precipitation of carbonates on tests might be interpreted as reduced/enhanced mass of planktic foraminiferal shells. Across all three western Mediterranean records (Fig. 1), scanning electron microscope images (Supplementary Figs. 5–7) of both species *G. bulloides* and *G. elongatus* show approximately the same degree of dissolution from top to bottom core depth with minor surface corrosion and breakup of the surface layer structure of the test wall^{67,68}. Therefore, calcite saturation level of subsurface to bottom waters at the three core sites are assumed to not have significantly changed, and weight loss of settling tests in the deep water column as discussed by Schiebel et al.⁶⁹ may have been the same over the entire time interval discussed here. As western Mediterranean deep and bottom waters are supersaturated with regard to calcite^{13,37,70}, dissolution at the sediment pore water interface is unlikely. The post-sapropel (<6 kyrs) western Mediterranean is a mesotrophic sea with limited changes and overall decreasing biological productivity over the past 150 years^{16,71}. Accordingly, supra-lysocline dissolution as well as corrosive porewater conditions, which may infer post depositional test weight reduction in surface seafloor sediments through decomposing organic matter can be assumed absent⁷². This is in line with previous sediment trap and core top studies from the western Mediterranean Sea, reporting no signs of dissolution in fossil planktic foraminifera assemblages^{32,33,73}. In contrast, early diagenetic calcite coating is reported for both species from core top samples at certain sites in the western and central Mediterranean Sea^{74,75}. However, no signs of diagenetic overgrowth and secondary precipitated inorganic carbonates (e.g., inorganic calcite crusts, inorganic calcite crystals, overgrown pores) are present in the tests of *G. elongatus* and *G. bulloides* from the three core sites analyzed here (Supplementary Figs. 5–7). Accordingly, due to the constant mild surface etching dissolution of similar magnitude of all tests observed across all three records, the relative foraminiferal SNW changes at the three core sites are expected to result from changes in biogenic calcification at the sea surface rather than diagenetic processes during sedimentation.

Driven by industrial carbon dioxide emissions, enhanced anthropogenic CO_2 penetration into the western Mediterranean Sea and resulting reductions in pH and $[\text{CO}_3^{2-}]$ are shown to be the key drivers of planktic foraminiferal SNW loss during the 20th century (Fig. 3a–f, Supplementary Fig. 2), corroborated by multiple regression analysis, discounting of multicollinearity

between the independent parameters controlling SNW changes (see methods). Reduced SNW of similar magnitude during the 20th century have been observed in the tropical Atlantic, Southern Ocean, the California Current System, and the western Mediterranean Sea, showing similar amplitudes of relative calcification decrease^{57,73,76,77}. Sea surface warming, productivity and solar activity changes are assumed to play only a negligible role, with rising SST and solar irradiance maxima potentially slightly attenuating the impact of anthropogenic CO₂ on planktic foraminiferal SNW. Accordingly, different oceanographic settings at the three selected core sites are responsible for the variability in 20th SNW trends (Supplementary Note 3), while the effects of diagenetic processes biasing the planktic foraminiferal SNW signal can be ruled out.

Conclusion

Accelerated anthropogenically-induced surface water pH decline in the western Mediterranean Sea is confirmed by boron isotopes and drives decreasing SNW of planktic foraminiferal tests. Negative carbon isotope excursions during the IE in tests of the planktic foraminifera species *G. elongatus* and *G. bulloides* display the signal of the Suess Effect—the anthropogenic CO₂-driven shift to lower δ¹³C—and highlight the influence of anthropogenic emissions as the most important driver of foraminiferal calcite mass decline. Alkenone-derived SST and instrumental temperature records show unprecedented anthropogenic sea surface warming, that potentially mitigates this effect slightly. This basin-wide, interspecies multiproxy approach, covering multidecadal to centennial time scales, thus yields a much-needed high-confidence, low-variability assessment of the impacts of anthropogenic climate change on key marine species, in a critically sensitive region.

Methods

Material. The study is based on high resolution multicore records collected in the central and western Mediterranean Sea with a MC400-Multicorer system during the MedSeA cruise (Mediterranean Sea Acidification in a changing climate) on 2nd May to 2nd June 2013 onboard the R/V Ángeles Alvariño. Core sampling of MedSeA-S3-c1 and MedSeA-S23-c1 was previously described in ref. ¹⁶. MedSeA-S7-c2 was retrieved in the Strait of Sicily (Lat. 37.7080° N, Long. 12.40553° E) at a water depth of 263 m, with a core length of 46.5 cm, sliced every centimeter.

Age Model development. Age models of cores MedSeA-S3-c1 and MedSeA-S23-c1 were estimated through a combination of radiocarbon and radionuclide dating, previously described in ref. ¹⁶. The age model of MedSeA-S7-c2 (Supplementary Table 2; Supplementary Note 4) was estimated through radionuclide analysis, determining total ²¹⁰Pb activity by measuring its alpha-emitter daughter nuclide ²¹⁰Po, following the methodology described in ref. ⁷⁸. ²⁰⁹Po was added as an internal tracer, before sample aliquots of 200–300 mg were totally digested in acid media by using an analytical microwave oven and Po isotopes plated on silver discs in HCl 1 N at 70 °C while stirring for 8 h. Po emissions were subsequently counted through α-spectrometers equipped with low background silicon surface barrier (SSB) detectors (EG&G Ortec) for 4 × 10⁵ seconds. The difference between total ²¹⁰Pb and the constant ²¹⁰Pb at depth describes the concentration of excess ²¹⁰Pb, which was used to estimate maximum mean sediment accumulation rates and the age-depth model by applying the Constant Flux: Constant Sedimentation (CF:CS) model^{79,80}. The activities of ¹³⁷Cs (661 keV) were determined by γ spectrometry in a coaxial high-purity Ge detector (EG&G Ortec) calibrated with the SRM-4276 solution standard supplied by the National Institute of Standards and Technology. The quality of the results determined by gamma and alpha spectrometry was evaluated by participation in IAEA proficiency tests and continuous analysis of certified and replicate materials.

Planktic foraminifera. Samples were dried at 60 °C for approximately 24 hours to obtain dry bulk sediment mass. After washing over a 63 μm screen using distilled Elux water, the size fraction larger than 63 μm was oven dried at 60 °C for 1–2 hours. Samples were dry sieved and divided by a riffle splitter (comparable to an ASC Sample Microsplitter, ASC Scientific) at the chosen size fractions: 150–250 μm, 250–315 μm, and > 315 μm. Total test accumulation rate was obtained by counting of more than 300 specimens in the >150 μm size fraction in all samples.

Taxonomic analysis of planktic foraminiferal tests was performed on core MedSeA-S7-c2 by visual identification using a binocular stereo microscope (magnification 10x–20x) and a bifurcated illuminator. Classification of

foraminiferal target species was based on⁴⁷, distinguishing between *Globigerina bulloides* (d'Orbigny 1826) and the two morphotypes of *Globigerinoides ruber* (d'Orbigny 1839), *Globigerinoides elongatus* and *G. ruber albus*⁸¹.

Size Normalized Weight. In order to obtain the calcite mass of planktic foraminiferal tests, a size related measure of test wall thickness and density—the Size Normalized Weight (SNW)—was obtained, which can be calculated by means of Eq. (1):

$$\text{SNW} = C + ((C * (100 - (100/B) * A)/100)) \quad (1)$$

Where C is the species average mass (μg) for each sample, A represents the average minimum Feret diameter (μm) for each sample and B is the average minimum Feret diameter (μm) of all specimens of one species of all samples. The equation (Eq. 1) includes the term to account for the relative SNW changes of the same species. Our methodology for measuring SNW is based on the sieve-based weight (SBW) technique, however, our approach also integrates measurements of individual test sizes in SNW estimations, a parameter used for the measurement-based weight (MBW) technique⁸². All specimens of a single sample are weighed together, while the average test size per sample is calculated by the minimum Feret diameter of each individual specimen. The SNW average standard deviation for each station (Alboran Sea: 7.0%; Balearic Sea: 8.3%; Strait of Sicily: 8.6%) is below the methodological 11% error reported by Beer, Schiebel⁸². Narrowing down the size fraction of analyzed tests to 250–315 μm ensured sufficient numbers of adult specimens which are large enough for SNW measurements. By applying the test weight size-normalization technique described above, we were able to factor out size related mass changes, mainly influenced by temperature variations.

SNW was determined for *G. elongatus* and *G. bulloides*. Bulk population measurements were performed on as many tests as available but not more than 10 and at least two specimens per sample per species, representing a total of 1,990 analyzed tests out of 224 samples included in this dataset. Selected tests were free of visible clay particles or organic matter and abnormally formed specimens were excluded from analysis. We weighed selected specimens together by triplicate with a Sartorius CP2P microbalance at Universitat Autònoma de Barcelona (UAB) and a Mettler Toledo XP6U Ultra Micro Balance at Max Planck Institute for Chemistry (MPIC) in Mainz, Germany, in environmentally controlled weighing rooms. Tests were positioned umbilical side up, photographed with a Canon EOS 650 D camera device attached to a Leica Z16 AP0 at UAB and with an Olympus UC90 attached to an Olympus SZY16 stereoscope at MPIC to measure the minimum Feret diameter of each individual test, using the software ImageJ 1.53k⁸³ and Olympus Stream Essentials 2.1. After measuring mean weight and mean minimum Feret diameter we calculated SNW for each sample using Eq. (1).

Biomarkers. Alkenones (heptatriaconta-8E,15E,22E-tri-2-one and heptatriaconta-15E,22E-di-2-one) of core MedSeA-S7-c2 were extracted from sediments, purified using organic solvents and quantified with a Varian gas chromatograph Model 450 equipped with a septum programmable injector, flame ionization detector and a CPSIL-5 CB column (coated with 100% dimethyl siloxane; film thickness of 0.12 μm; L(m) * ID(mm) * OD(mm): 50 * 0.32 * 0.45). Hydrogen was the carrier gas (2.5 mL min⁻¹). Concentrations were determined using n-hexatriacontane (CH₃(CH₂)₃₄CH₃) as an internal standard. Absolute concentration errors were below 10% (resolution between the alkenones from 1.5 to 1.7). Reproducibility tests showed that uncertainty in the U^k₃₇ determination is lower than 0.015 (ca. 0.5 °C)¹⁶, this study, ^{84–86} confirming the precision of the paleothermometry tool⁸⁷. SST reconstructions were based on the global calibration of Conte, Sicre⁸⁸, with a standard error on surface sediments at 1.1 °C.

Stable isotope measurements. For chemical analysis, adult specimens were selected from a narrow size range (250–315 μm) to minimize uncertainty in paleoceanographic interpretation due to vital effects, following suggestions by Spero and Lea⁸⁹.

δ¹³C and δ¹⁸O. Bulk population measurements, including 5–10 specimens per species sample (not necessarily the same specimens as used for SNW measurements), were performed on *G. elongatus* and *G. bulloides*. Sample weight was determined through a Mettler Toledo XP6U Ultra Micro Balance at MPIC. Selected tests were crushed and soaked in ultrapure water (Milli-Q), before ultrasonication for up to 20 seconds, to remove clay contamination.

Samples were analyzed on a Thermo Delta V mass spectrometer equipped with a GASBENCH preparation device. ~8–50 μg of CaCO₃ sample, placed in a He-filled 4.5 ml exetainer vial was digested in water-free H₃PO₄ at a temperature of 70 °C. Subsequently the CO₂-He gas mixture was transported to the GASBENCH in Helium carrier gas. In the GASBENCH, water vapor and various gaseous compounds were separated from the He-CO₂ mixture prior to sending it to the mass spectrometer in nine separate peaks. Isotope values of these individual peaks were averaged and reported as δ¹³C and δ¹⁸O relative to V-PDB. A total of 20 replicates of two in-house CaCO₃ standards were analyzed in each run of 55 samples. CaCO₃ standard weights were chosen so that they span the entire range of sample weights of the samples. After correction of isotope effects related to

sample size the reproducibility of these standards is typically better than 0.1 ‰ (1 SD) for $\delta^{18}\text{O}$ and 0.1 ‰ (1 SD) for $\delta^{13}\text{C}$.

Samples of 8 to 3 μg of CaCO_3 were analyzed on the same equipment using a cold trap technique that analyzes the entire sample in one single peak^{90,91}. With this setting, 30 CaCO_3 standards were analyzed in each run of 30 samples. CaCO_3 standard weights were chosen so that they span the entire range of sample weights of the samples. Reproducibility of these <8 μg standards with the cold trap technique, after sample size correction, is typically better than 0.1 ‰ (1 SD) for $\delta^{18}\text{O}$ and 0.1 ‰ (1 SD) for $\delta^{13}\text{C}$.

$\delta^{11}\text{B}$. For boron isotope analysis, samples of *G. ruber* (250–315 μm) were prepared in a class 100 clean lab at the University of St Andrews STAiG laboratories. The two morphotypes of the species were analyzed separately. Samples were first crushed between two glass slides before transferring to acid cleaned centrifuge tubes in preparation for clay removal by ultrasonication. This was followed by oxidative cleaning in 1% hydrogen peroxide buffered with 0.1 M NH_4OH and a weak acid leach in 0.0005 M distilled HNO_3 according to established protocols^{92,93}. After addition of 100 μl boron-free Milli-Q, samples were dissolved by incremental addition of 0.5 M distilled HNO_3 (total volume of acid per sample 30–50 μl). A 5% cut of the dissolved sample was analyzed by ICP-MS for a suite of trace elements (Supplementary Table 3) including Mg/Ca on an Agilent 8900 following Foster⁹⁴ and Rae, Foster⁹⁵ with the addition of trace hydrofluoric acid in the wash to improve washout⁹⁵. Samples were run alongside matrix-matched bracketing and consistency standards to monitor long-term instrument reproducibility which is reported at 95% confidence (2 SD). Low Al/Ca in all samples confirms the absence of residual clays. Elevated Mn/Ca was recorded in one sample but it does not display elevated Mg/Ca or any other anomalous trace element or isotopic signal.

After trace element analysis, a few samples with low boron concentrations, as determined from B/Ca, meant it was necessary to combine adjacent dissolved samples in MedSea-S7-c2 core in order to reduce $\delta^{11}\text{B}$ uncertainty (Supplementary Table 4). Boron was isolated from the sample matrix using boron-specific Amberlite IRA 743 resin^{96,97} using a batch method. For this technique, 2 ml centrifuge tubes containing 50 μl of resin were pre-cleaned by addition and removal of 1 ml 0.5 M HNO_3 (repeated 3 times) and 1 ml boron-free Milli-Q (repeated twice) and then pre-conditioned with 100 μl 0.1 M ammonium acetate buffer at pH 8.5. Before loading, the sample was first buffered to pH 5 with 0.1 M ammonium acetate. After pipetting onto the resin, the tubes were agitated on a VWR mini vortex and the solution pipetted off after the resin settled. Following rinses with boron free Milli-Q water, the concentrated sample was eluted in 500 μl 0.5 M distilled HNO_3 and the boron isotopic composition analyzed by MC-ICPMS with sample-standard bracketing against NIST 951 according to methods described by^{93,94}. Addition of Hydrofluoric acid at 0.3 M helped to improve washout and reduce boron evaporation⁹⁵. Matrix matched carbonate consistency standards were run alongside samples to monitor reproducibility which is ± 0.23 ‰ (2 SD).

pH Calculations

CO2SYS. To estimate unknown variables in the seawater marine carbonate system, we used the CO2SYS program (version 2.0)⁹⁸. Through a set of given input conditions (e.g., temperature, salinity, atm. CO_2 concentration), this program can estimate the remaining unknown variables of a two “master” carbonate system (TA, DIC, pH, pCO_2). We estimated surface ocean pH and carbonate ion concentrations for the three study sites, using seawater pCO_2 and total alkalinity (TA). TA was assumed constant over the last century, accounting for 2400 $\mu\text{mol/kgSW}$ in the Alboran Sea⁹⁹, 2478 $\mu\text{mol/kgSW}$ in the Strait of Sicily¹³, and 2550 $\mu\text{mol/kgSW}$ in the Balearic Sea¹⁰⁰. Surface seawater pCO_2 was derived from temperature, salinity and pressure dependent solubility coefficient (K_0) following the formulation of Weiss¹⁰¹ and atmospheric CO_2 measurements from an interpolated stack including the Mauna Loa time series¹⁰² and reconstructed CO_2 concentrations^{103,104}. Time-specific K_0 values were determined as input conditions for down core calculations using surface pressure, SST and salinity for each study location. SST was based on alkenone ($U^{k_{37}}$) derived paleo estimates at each study location^{16,105} and salinity was defined as the constant mean (1950–2019 CE) of Hadley EN4 (version EN.4.2.2) subsurface salinity objective analysis¹⁰⁶. Constants for our CO2SYS carbonate system estimations were the dissociation constant (K_1 and K_2) defined by¹⁰⁷, refitted to seawater scale by¹⁰⁸, the dissociation constants K_{HSO_4} and K_B according to¹⁰⁹, and the chlorinity relationship and boron concentration based on¹¹⁰.

Boron isotope transformation. To calculate pH, the $\delta^{11}\text{B}$ of *G. ruber albus* and *G. elongatus* was first converted to seawater $\delta^{11}\text{B}_{\text{borate}}$ using the calibration of¹¹¹ for the 250 – 300 μm size fraction:

$$\delta^{11}\text{B}_{\text{borate}} = (\delta^{11}\text{B}_{\text{foram}} - 9.52 \pm 1.51) / (0.60 \pm 0.08) \quad (2)$$

The boric acid dissociation constant is determined by both salinity and temperature and thus calculated pH can be susceptible to variations in these assigned values. Salinity was set at modern levels (37 PSU) for the region and temperature was calculated from Mg/Ca using the species specific calibration for *G. ruber* from¹¹².

$$\text{Mg/Ca} = 0.97 \pm 0.50 \times \exp(0.063 \pm 0.019 \times T) \quad (3)$$

The pH derived from Mg/Ca temperatures were compared to those from temperatures determined from Hadley, $U^{k_{37}}$ and $\delta^{18}\text{O}$ SST in (Supplementary Table 4). A sample depth of 25 m was given to approximate the upper habitation depth of the species below the sea surface³¹.

Statistical analysis

General additive model. Statistical analysis has been performed using the statistical software R¹¹³. General additive models (GAM) have been used in paleoenvironmental time series as a superior alternative tool to conventional statistical trend estimations¹¹⁴. We used a GAM to better show the basin wide, interspecies specific change in SNW and $\delta^{13}\text{C}$, and western Mediterranean SST changes. The complex, non-linear GAM fits as a smoothed function, which allows us to identify the period of significant SNW, $\delta^{13}\text{C}$ and SST change based on proper accounting for model uncertainty. The general and applied mathematical form of the general additive model can be described as:

$$y_i = \beta_0 + f(x_i) + \varepsilon_i \text{ where } \varepsilon_i \sim N(0, \sigma^2) \quad (4)$$

$$\text{SNW} = 4.081e^{-15} + 6.997 + \varepsilon_i \text{ where } \varepsilon_i \sim N(0, \sigma^2) \quad (5)$$

$$\delta^{13}\text{C} = 0.02111 + 6.238 + \varepsilon_i \text{ where } \varepsilon_i \sim N(0, \sigma^2) \quad (6)$$

$$\text{SST} = -0.02993 + 8.033 + \varepsilon_i \text{ where } \varepsilon_i \sim N(0, \sigma^2) \quad (7)$$

SNW and $\delta^{13}\text{C}$ values were standardized and merged, combining *G. bulloides* and *G. elongatus* at all three stations. Standardized SST is based on alkenone measurements and the calculated mean from HadISST dataset across the three stations. Uncertainty in the estimated model fits were addressed through 95% confidence intervals, after confirming gaussian error distribution via histogram plot, Q-Q plot and Kolmogorov-Smirnov test for standardized datasets of SNW (p -value = 0.5501), $\delta^{13}\text{C}$ (p -value = 0.1738) and SST (p -value = 0.7126). Additionally, a GAM fit was applied¹¹⁵, by means of the *mgcv* package (version 1.8.42). To avoid under smoothing of the fit, the smoothing term was calculated using restricted maximum likelihood^{116,117}.

Regression analysis. To quantify changes of SNW and $\delta^{13}\text{C}$ during the 20th century, linear regression analysis was applied including all available data points post 1900 CE. Estimations of SNW and $\delta^{13}\text{C}$ (negative anthropogenic carbon isotope excursions; nCIEs) change are defined by the difference between 1900 CE and 2013 CE, based on the regression model accounting for statistical significance (Supplementary Figs. 1, 2). To determine statistically significant relationships between the explanatory variable (SNW) and the independent variables (productivity, SST, pH and $\delta^{13}\text{C}$) we performed multiple linear regression analysis for time windows prior (pre-Industrial Era) and post 1800 CE (Industrial Era). Abundance changes of indicator species, along with changes in alkenone concentrations and planktic foraminiferal test accumulation rates (Fig. 2b) are included in the productivity variable. SST changes are based on the alkenone and HadISST datasets (Fig. 2a). The pH variability is calculated from pCO_2 and total alkalinity on CO2SYS (Fig. 2d), and $\delta^{13}\text{C}$ changes are based on carbon isotope measurements (Fig. 2c). To generate evenly spaced time series, we standardized data for each station and parameter before combining station data for each parameter by interpolating non-linear GAM fits (method see above) using generalized cross-validation (GCV) method for smoothing parameter estimation to avoid over smoothing of the fit. Goodness of the fit for each parameter is shown through deviance explained (Supplementary Table 5). Due to high collinearity, we have removed pH from the model including data post 1800 CE. Both parameters are highly correlated particularly during the Industrial Era as the $\delta^{13}\text{C}$ signals mirrors the input of anthropogenic CO_2 , resulting in pH decrease (see discussion). The conditions of application required for the multiple linear regression analysis have been verified by using *performance* package (version 0.10.3). It can be assumed that there is no problematic amount of Multicollinearity since all parameters included in the model show a Variance Inflation Factor below ten¹¹⁸. Information on multiple linear regression models and their significance values can be found in the supplementary material (Supplementary Tables 6, 7), confirming a significant correlation between independent parameters and the explanatory variable, and substantiating the effect of ocean acidification on SNW.

Reporting summary. Further information on research design is available in the Nature Portfolio Reporting Summary linked to this article.

Data availability

The dataset used in this study is publicly available online for download at PANGAEA Data Publisher (<https://doi.org/10.1594/PANGAEA.955024>).

Received: 18 November 2022; Accepted: 28 July 2023;

Published online: 28 August 2023

References

- Jacobson, M. Z., Studying ocean acidification with conservative, stable numerical schemes for nonequilibrium air-ocean exchange and ocean equilibrium chemistry. *J. Geophys. Res.* **110**, 1–17 (2005).
- Orr, J. C. et al. Anthropogenic ocean acidification over the twenty-first century and its impact on calcifying organisms. *Nature* **437**, 681–686 (2005).
- Kroeker, K. J. et al. Impacts of ocean acidification on marine organisms: quantifying sensitivities and interaction with warming. *Glob. Chang. Biol.* **19**, 1884–1896 (2013).
- NOAA National Centers for Environmental Information. *State of the Climate: Global Climate Report for Annual 2020*. (2021). <https://www.ncdc.noaa.gov/sotc/global/202013>.
- Abram, N. J. et al. Early onset of industrial-era warming across the oceans and continents. *Nature* **536**, 411 (2016).
- Li, G. et al. Increasing ocean stratification over the past half-century. *Nat. Clim. Chang.* **10**, 1116–1123 (2020).
- Behrenfeld, M. J. et al. Climate-driven trends in contemporary ocean productivity. *Nature* **444**, 752–755 (2006).
- Weinkauff, M. F. G. et al. Seasonal variation in shell calcification of planktonic foraminifera in the NE Atlantic reveals species-specific response to temperature, productivity, and optimum growth conditions. *PLoS ONE* **11**, e0148363 (2016).
- Marshall, B. J. et al. Planktonic foraminiferal area density as a proxy for carbonate ion concentration: A calibration study using the Cariaco Basin ocean time series. *Paleoceanography* **28**, 363–376 (2013).
- Giorgi, F. Climate change hot-spots. *Geophys. Res. Lett.* **33**, 1–4 (2006).
- Cramer, W. et al. Climate change and interconnected risks to sustainable development in the Mediterranean. *Nature Climate Change* **8**, 972–980 (2018).
- Schneider, A. et al. High anthropogenic carbon content in the eastern Mediterranean. *J. Geophys. Res.* **115**, 1–11 (2010).
- Schneider, A., Wallace, D. W., and Körtzinger, A., Alkalinity of the Mediterranean sea. *Geophys. Res. Lett.* **34**, 1–5 (2007).
- Touratier, F. & Goyet, C. Decadal evolution of anthropogenic CO₂ in the northwestern Mediterranean Sea from the mid-1990s to the mid-2000s. *Deep Sea Res. Part I* **56**, 1708–1716 (2009).
- Shaltout, M. & Omstedt, A. Recent sea surface temperature trends and future scenarios for the Mediterranean Sea. *Oceanologia* **56**, 411–443 (2014).
- Pallacks, S. et al. Planktic foraminiferal changes in the western Mediterranean Anthropocene. *Glob. Planet. Chang.* **204**, 103549 (2021).
- Richardson, A. J. et al. Using continuous plankton recorder data. *Prog. Oceanogr.* **68**, 27–74 (2006).
- Bates, N. R. et al. A Time-Series View of Changing Surface Ocean Chemistry Due to Ocean Uptake of Anthropogenic CO₂ and Ocean Acidification. *Oceanography* **27**, 126–141 (2014).
- Madrid, C. R., *The Nimbus 7 User's Guide*. (ed. Madrid, C. R) 263 (Greenbelt, Maryland, NASA Goddard Space Flight Center, 1978).
- Henson, S. A. et al. Detection of anthropogenic climate change in satellite records of ocean chlorophyll and productivity. *Biogeosciences* **7**, 621–640 (2010).
- Pisano, A. et al. New Evidence of Mediterranean Climate Change and Variability from Sea Surface Temperature Observations. *Remote Sens.* **12**, 132 (2020).
- Lionello, P. et al. *The Mediterranean climate: An overview of the main characteristics and issues*, in *Developments in Earth and Environmental Sciences*. (eds. Lionello, P., Malanotte-Rizzoli, P., Boscolo, R). 1–26, (Elsevier, 2006).
- Marriner, L. et al. Anthropocene tipping point reverses long-term Holocene cooling of the Mediterranean Sea: A meta-analysis of the basin's Sea Surface Temperature records. *Earth-Sci. Rev.* **227**, 1–11 (2022).
- Schiebel, R. Planktic foraminiferal sedimentation and the marine calcite budget. *Glob. Biogeochem. Cycles* **16**, 3–13-21 (2002).
- Raja, M. & Rosell-Melé, A. Appraisal of sedimentary alkenones for the quantitative reconstruction of phytoplankton biomass. *Proc. Natl Acad. Sci.* **118**, e2014787118 (2021).
- Macias, D. M. et al. Biogeochemical control of marine productivity in the Mediterranean Sea during the last 50 years. *Glob. Biogeochem. Cycles* **28**, 897–907 (2014).
- Boyce, D. G. et al. Estimating global chlorophyll changes over the past century. *Prog. Oceanogr.* **122**, 163–173 (2014).
- Quay, P. D., Tilbrook, B. & Wong, C. S. Oceanic Uptake of Fossil Fuel CO₂: Carbon-13 Evidence. *Science* **256**, 74–79 (1992).
- Eide, M. et al. A global estimate of the full oceanic 13C Suess effect since the preindustrial. *Glob. Biogeochem. Cycles* **31**, 492–514 (2017).
- Mellon, S. et al. Foraminifera Trace Anthropogenic CO₂ in the NW Atlantic by 1950. *Geophys. Res. Lett.* **46**, 14683–14691 (2019).
- Pujol, C. & Grazzini, C. V. Distribution patterns of live planktic foraminifera as related to regional hydrography and productive systems of the Mediterranean Sea. *Marine Micropaleontol.* **25**, 187–217 (1995).
- Bárcena, M. A. et al. Planktonic response to main oceanographic changes in the Alboran Sea (Western Mediterranean) as documented in sediment traps and surface sediments. *Marine Micropaleontol.* **53**, 423–445 (2004).
- Rigual-Hernández, A. S. et al. Seasonal and interannual changes of planktic foraminiferal fluxes in the Gulf of Lions (NW Mediterranean) and their implications for paleoceanographic studies: two 12-year sediment trap records. *Deep Sea Res. Part I* **66**, 26–40 (2012).
- Gruber, N. et al. Spatiotemporal patterns of carbon-13 in the global surface oceans and the oceanic suess effect. *Glob. Biogeochem. Cycles* **13**, 307–335 (1999).
- Caldeira, K. & Wickett, M. E. Anthropogenic carbon and ocean pH. *Nature* **425**, 365–365 (2003).
- Hassoun, A. E. R. et al. Ocean acidification research in the Mediterranean Sea: Status, trends and next steps. *Front. Marine Sci.* **9**, 1–28 (2022).
- Álvarez, M. et al. The CO₂ system in the Mediterranean Sea: a basin wide perspective. *Ocean Sci.* **10**, 69–92 (2014).
- Jiménez-López, D. et al. Aragonite saturation state in a continental shelf (Gulf of Cádiz, SW Iberian Peninsula): Evidence of acidification in the coastal area. *Sci. Total Environ.* **787**, 1–15 (2021).
- Marcellin Yao, K. et al. Time variability of the north-western Mediterranean Sea pH over 1995–2011. *Marine Environ. Res.* **116**, 51–60 (2016).
- Kapsenberg, L. et al. Coastal ocean acidification and increasing total alkalinity in the northwestern Mediterranean Sea. *Ocean Sci.* **13**, 411–426 (2017).
- Flecha, S. et al. Decadal acidification in Atlantic and Mediterranean water masses exchanging at the Strait of Gibraltar. *Sci. Rep.* **9**, 15533 (2019).
- Hassoun, A. E. R. et al. Acidification of the Mediterranean Sea from anthropogenic carbon penetration. *Deep Sea Res. Part I* **102**, 1–15 (2015).
- Gehlen, M. et al. Section 2.10: Ocean acidification, in *Copernicus Marine Service Ocean State Report, Issue 4, Journal of Operational Oceanography*. (eds. K. von Schuckmann and P.-Y. Le Traon) 64–76. (2020).
- Spero, H. J. et al. Effect of seawater carbonate concentration on foraminiferal carbon and oxygen isotopes. *Nature* **390**, 497 (1997).
- Peeters, F. J. C., Brummer, G.-J. A. & Ganssen, G. The effect of upwelling on the distribution and stable isotope composition of Globigerina bulloides and Globigerinoides ruber (planktic foraminifera) in modern surface waters of the NW Arabian Sea. *Glob. Planet. Chang.* **34**, 269–291 (2002).
- Bijma, J., H. J. Spero, and D. W. Lea, Reassessing Foraminiferal Stable Isotope Geochemistry: Impact of the Oceanic Carbonate System (Experimental Results), in *Use of Proxies in Paleoceanography: Examples from the South Atlantic*. (eds. Fischer G., Wefer, G.) 489–512 (Berlin, Heidelberg, Springer Berlin Heidelberg, 1999).
- Schiebel, R. and C. Hemleben, *Planktic foraminifera in the modern ocean*. (Berlin, Heidelberg, Springer, 2017).
- Köhler-Rink, S. & Kühl, M. The chemical microenvironment of the symbiotic planktonic foraminifer *Orbulina universa*. *Marine Biol. Res.* **1**, 68–78 (2005).
- Spero, H. J. Do planktic foraminifera accurately record shifts in the carbon isotopic composition of seawater ΣCO_2 ? *Marine Micropaleontol.* **19**, 275–285 (1992).
- Bird, C. et al. Cyanobacterial endobionts within a major marine planktonic calcifier (Globigerina bulloides, Foraminifera) revealed by 16S rRNA metabarcoding. *Biogeosciences* **14**, 901–920 (2017).
- Osborne, E. B. et al. Calcification of the planktonic foraminifera Globigerina bulloides and carbonate ion concentration: Results from the Santa Barbara Basin. *Paleoceanography* **31**, 1083–1102 (2016).
- Keul, N. et al. Effect of ocean acidification on the benthic foraminifera *Ammonia* sp. is caused by a decrease in carbonate ion concentration. *Biogeosciences* **10**, 6185–6198 (2013).
- Dong, S. et al. Biological Response of Planktic Foraminifera to Decline in Seawater pH. *Biology* **11**, 98 (2022).
- Beer, C. J., Schiebel, R. & Wilson, P. A. Testing planktic foraminiferal shell weight as a surface water [CO₃²⁻] proxy using plankton net samples. *Geology* **38**, 103–106 (2010).
- Doney, S. C. et al. Ocean Acidification: The Other CO₂ Problem. *Annu. Rev. Marine Sci.* **1**, 169–192 (2009).
- Davis, C. V. et al. Ocean acidification compromises a planktic calcifier with implications for global carbon cycling. *Sci. Rep.* **7**, 2225–2225 (2017).
- Moy, A. D. et al. Reduced calcification in modern Southern Ocean planktonic foraminifera. *Nat. Geosci.* **2**, 276 (2009).
- Aldridge, D., Beer, C. J. & Purdie, D. A. Calcification in the planktonic foraminifera Globigerina bulloides linked to phosphate concentrations in surface waters of the North Atlantic Ocean. *Biogeosciences* **9**, 1725–1739 (2012).
- Naik, S. S., Godad, S. P. & Naidu, P. D. Does carbonate ion control planktonic foraminifera shell calcification in upwelling regions? *Curr. Sci.* **101**, 1370–1375 (2011).
- Todd, C. L. et al. Planktic Foraminiferal Test Size and Weight Response to the Late Pliocene Environment. *Paleoceanogr. Paleoclimatol.* **35**, e2019PA003738 (2020).

61. Spero, H. J., Lerche, I. & Williams, D. F. Opening the carbon isotope ‘vital effect’ black box, 2, Quantitative model for interpreting foraminiferal carbon isotope data. *Paleoceanography* **6**, 639–655 (1991).
62. Gonzalez-Mora, B., Sierro, F. & Flores, J. Controls of shell calcification in planktonic foraminifers. *Quat. Sci. Rev.* **27**, 956–961 (2008).
63. Mallo, M. et al. Low planktic foraminiferal diversity and abundance observed in a spring 2013 west-east Mediterranean Sea plankton tow transect. *Biogeosciences*, **14**, 2245–2266 (2017).
64. de Nooijer, L. J. et al. Biomineralization in perforate foraminifera. *Earth-Sci. Rev.* **135**, 48–58 (2014).
65. Hemleben, C., M. Spindler, & Anderson, O. R. *Modern planktonic foraminifera*. (New York, NY, Springer, 1989).
66. Schiebel, R. & Hemleben, C. Modern planktic foraminifera. *Paläontologische Zeitschrift* **79**, 135–148 (2005).
67. Dittert, N. & Henrich, R. Carbonate dissolution in the South Atlantic Ocean: evidence from ultrastructure breakdown in Globigerina bulloides. *Deep Sea Res. Part I* **47**, 603–620 (2000).
68. Regenberg, M. et al. WEIGHT LOSS AND ELIMINATION OF PLANKTONIC FORAMINIFERAL TESTS IN A DISSOLUTION EXPERIMENT. *J. Foraminif. Res.* **43**, 406–414 (2013).
69. Schiebel, R. et al. Planktic foraminiferal dissolution in the twilight zone. *Deep Sea Res. Part II* **54**, 676–686 (2007).
70. Millero, F. J., Morse, J. & Chen, C.-T. The carbonate system in the western Mediterranean Sea. *Deep Sea Res. Part A* **26**, 1395–1404 (1979).
71. Jimenez-Espejo, F. J. et al. Detrital input, productivity fluctuations, and water mass circulation in the westernmost Mediterranean Sea since the Last Glacial Maximum. *Geochem. Geophys. Geosyst.* **9**, 1–19 (2008).
72. Tachikawa, K. et al. Assessing influence of diagenetic carbonate dissolution on planktonic foraminiferal Mg/Ca in the southeastern Arabian Sea over the past 450 ka: Comparison between Globigerinoides ruber and Globigerinoides sacculifer. *Geochem. Geophys. Geosyst.* **9**, 1–16 (2008).
73. Béjard, T. M. et al. Calcification response of planktic foraminifera to environmental change in the western Mediterranean Sea during the industrial era. *Biogeosciences* **20**, 1505–1528 (2023).
74. Sabbatini, A. et al. Further constraints on the diagenetic influences and salinity effect on Globigerinoides ruber (white) Mg/Ca thermometry: Implications in the Mediterranean Sea. *Geochem. Geophys. Geosyst.* **12**, 1–19 (2011).
75. Van Raden, U. J. et al. Mg/Ca in the planktonic foraminifera Globorotalia inflata and Globigerinoides bulloides from Western Mediterranean plankton tow and core top samples. *Marine Micropaleontol.* **78**, 101–112 (2011).
76. Davis, A. N. et al. Reconstructing 800 Years of Carbonate Ion Concentration in the Cariaco Basin Using the Area Density of Planktonic Foraminifera Shells. *Paleoceanogr. Paleoclimatol.* **34**, 2129–2140 (2019).
77. Osborne, E. B. et al. Decadal variability in twentieth-century ocean acidification in the California Current Ecosystem. *Nature Geoscience* **13**, 43–49 (2020).
78. Sánchez-Cabeza, J., Masqué, P. & Ani-Ragolta, I. 210Pb and 210Po analysis in sediments and soils by microwave acid digestion. *J. Radioanal. Nuclear Chem.* **227**, 19–22 (1998).
79. Krishnaswamy, S. et al. Geochronology of lake sediments. *Earth Planet. Sci. Lett.* **11**, 407–414 (1971).
80. Robbins, J. A., Geochemical and geophysical applications of radioactive lead, in *Biogeochemistry of Lead in the Environment*. (ed. Nriagu, J. O.) 285–393. (Amsterdam, Elsevier Scientific, 1978).
81. Morard, R. et al. Genetic and morphological divergence in the warm-water planktonic foraminifera genus Globigerinoides. *PLOS ONE* **14**, e0225246 (2019).
82. Beer, C. J., Schiebel, R. & Wilson, P. On methodologies for determining the size-normalised weight of planktic foraminifera. *Biogeosciences* **7**, 2193 (2010).
83. Schneider, C. A., Rasband, W. S. & Eliceiri, K. W. NIH Image to ImageJ: 25 years of image analysis. *Nat. Methods* **9**, 671–675 (2012).
84. Cacho, I. et al. Dansgaard-Oeschger and Heinrich event imprints in Alboran Sea paleotemperatures. *Paleoceanogr. Paleoclimatol.* **14**, 698–705 (1999).
85. Martrat, B. et al. Abrupt temperature changes in the Western Mediterranean over the past 250,000 years. *Science* **306**, 1762–1765 (2004).
86. Martrat, B. et al. Similarities and dissimilarities between the last two deglaciations and interglaciations in the North Atlantic region. *Quat. Sci. Rev.* **99**, 122–134 (2014).
87. Eglinton, T. I. et al. Proceedings of a workshop on alkenone-based paleoceanographic indicators. *Geochem. Geophys. Geosyst.* **2** (2001).
88. Conte, M. H. et al. Global temperature calibration of the alkenone unsaturation index (UK’ 37) in surface waters and comparison with surface sediments. *Geochem. Geophys. Geosyst.* **7**, 1–22 (2006).
89. Spero, H. J. & Lea, D. W. Experimental determination of stable isotope variability in Globigerina bulloides: implications for paleoceanographic reconstructions. *Marine Micropaleontol.* **28**, 231–246 (1996).
90. Fiebig, J., Schöne, B. R. & Oschmann, W. High-precision oxygen and carbon isotope analysis of very small (10–30 µg) amounts of carbonates using continuous flow isotope ratio mass spectrometry. *Rapid Commun. Mass Spectrom.* **19**, 2355–2358 (2005).
91. Vonhof, H. B. et al. High-precision stable isotope analysis of <5 µg CaCO₃ samples by continuous-flow mass spectrometry. *Rapid Commun. Mass Spectrom.* **34**, e8878 (2020).
92. Barker, S., M. Greaves, and H. Elderfield, A study of cleaning procedures used for foraminiferal Mg/Ca paleothermometry. *Geochem. Geophys. Geosyst.* **4**, 1–20 (2003).
93. Rae, J. W. B. et al. Boron isotopes and B/Ca in benthic foraminifera: Proxies for the deep ocean carbonate system. *Earth Planet. Sci. Lett.* **302**, 403–413 (2011).
94. Foster, G. L. Seawater pH, pCO₂ and [CO₂-3] variations in the Caribbean Sea over the last 130 kyr: A boron isotope and B/Ca study of planktic foraminifera. *Earth Planet. Sci. Lett.* **271**, 254–266 (2008).
95. Zeebe, R. E. & Rae, J. W. B. Equilibria, kinetics, and boron isotope partitioning in the aqueous boric acid–hydrofluoric acid system. *Chem. Geol.* **550**, 119693 (2020).
96. Kiss, E. Ion-exchange separation and spectrophotometric determination of boron in geological materials. *Anal. Chim. Acta* **211**, 243–256 (1988).
97. Lemarchand, D. et al. Boron isotope systematics in large rivers: Implications for the marine boron budget and paleo-pH reconstruction over the Cenozoic. *Chem. Geol.* **190**, 123–140 (2002).
98. Lewis, E., Wallace, D. & Allison, L. J. Program developed for CO₂ system calculations. <https://doi.org/10.2172/639712> (Oak Ridge National Laboratory, United States, 1998).
99. Cossarini, G., Lazzari, P., and Solidoro, C., Spatiotemporal variability of alkalinity in the Mediterranean Sea. *Biogeosciences*, **12**, 1647–1658 (2015).
100. Gemayel, E. et al. Climatological variations of total alkalinity and total inorganic carbon in the Mediterranean Sea surface waters. *Earth Syst. Dynam.* **6**, 789–800 (2015).
101. Weiss, R. F. Carbon dioxide in water and seawater: the solubility of a non-ideal gas. *Marine Chem.* **2**, 203–215 (1974).
102. Tans, P. & Keeling, R. F. *Trends in Atmospheric Carbon Dioxide*. 2020. <https://www.esrl.noaa.gov/gmd/ccgg/trends/data.html>.
103. Friedli, H. et al. Ice core record of the 13C/12C ratio of atmospheric CO₂ in the past two centuries. *Nature* **324**, 237–238 (1986).
104. Bauska, T. K. et al. Links between atmospheric carbon dioxide, the land carbon reservoir and climate over the past millennium. *Nat. Geosci.* **8**, 383–387 (2015).
105. Incarbona, A. et al. Mediterranean circulation perturbations over the last five centuries: Relevance to past Eastern Mediterranean Transient-type events. *Sci. Rep.* **6**, 1–10 (2016).
106. Good, S. A., Martin, M. J. & Rayner, N. A. EN4: Quality controlled ocean temperature and salinity profiles and monthly objective analyses with uncertainty estimates. *J. Geophys. Res.* **118**, 6704–6716 (2013).
107. Mehrbach, C. et al. Measurement of the apparent dissociation constants of carbonic acid in seawater at atmospheric pressure. *Limnol. Oceanogr.* **18**, 897–907 (1973).
108. Dickson, A. G. & Millero, F. J. A comparison of the equilibrium constants for the dissociation of carbonic acid in seawater media. *Deep Sea Res. Part A. Oceanogr. Res. Papers* **34**, 1733–1743 (1987).
109. Dickson, A. G. Standard potential of the reaction: AgCl(s) + 12H₂(g) = Ag(s) + HCl(aq), and the standard acidity constant of the ion HSO₄[–] in synthetic sea water from 273.15 to 318.15 K. *J. Chem. Thermodynam.* **22**, 113–127 (1990).
110. Uppstrom, L. R. The boron/chlorinity ratio of deep-sea water from the Pacific Ocean. *Deep Sea Res.* **21**, 161–162 (1974).
111. Henehan, M. J. et al. Calibration of the boron isotope proxy in the planktonic foraminifera Globigerinoides ruber for use in palaeo-CO₂ reconstruction. *Earth Planet. Sci. Lett.* **364**, 111–122 (2013).
112. Gray, W. R. et al. The effects of temperature, salinity, and the carbonate system on Mg/Ca in Globigerinoides ruber (white): A global sediment trap calibration. *Earth Planet. Sci. Lett.* **482**, 607–620 (2018).
113. R Core Team, R: A Language and Environment for Statistical Computing, R Foundation for Statistical Computing: Vienna, Austria (2023).
114. Simpson, G. L., Modelling Palaeoecological Time Series Using Generalised Additive Models. *Front. Ecol. Evol.* **6**, 1–21 (2018).
115. Wood, S. N. Fast stable restricted maximum likelihood and marginal likelihood estimation of semiparametric generalized linear models. *J. R. Stat. Soc.* **73**, 3–36 (2011).
116. Wood, S. N., Pya, N. & Säfken, B. Smoothing Parameter and Model Selection for General Smooth Models. *J. Am. Stat. Assoc.* **111**, 1548–1563 (2016).
117. Reiss, P. T. & Todd Ogden, R. Smoothing parameter selection for a class of semiparametric linear models. *J. R. Stat. Soc.* **71**, 505–523 (2009).
118. James, G. et al. Linear Regression, in *An Introduction to Statistical Learning: with Applications in R*. 59–126 (New York, NY, Springer New York, 2013).
119. Garcia, H. et al. World Ocean Atlas 2018: Product Documentation. (ed. Mishonov, A.) <https://www.ncei.noaa.gov/data/oceans/wao/WOA18/DOC/wao18documentation.pdf> (2019).

120. Gregor, L. & Gruber, N. OceanSODA-ETHZ: a global gridded data set of the surface ocean carbonate system for seasonal to decadal studies of ocean acidification. *Earth Syst. Sci. Data* **13**, 777–808 (2021).
121. Schlitzer, R., *Ocean Data View*. <https://odv.awi.de/> (2023).
122. Pallacks, S. et al. Age model, sea surface temperature and marine calcifying plankton changes at two sites in the western Mediterranean Sea for the Common Era., PANGAEA (2021).

Acknowledgements

We are grateful to Manuel F. G. Weinkauff, Laura Haynes and an anonymous reviewer for their helpful comments and suggestions. We thank the captain and crew of the Spanish R/V Angeles Alvarino, and the researchers as part of the MedSeA cruise for supporting the sampling of this study. We also thank Marta Casado, Yolanda Gonzalez-Quinteiro and Natalia Bravo for laboratory assistance, and Joan Manuel Bruach for his work on the analysis of ^{210}Pb . This work contributes to the ICTA-UAB “Unit of Excellence” (FPI/MDM-2015-0552- 16-2; CEX2019-000940-M) and was funded by the Spanish Ministry of Science and Innovation, BIOCAL Project (PID2020-113526RB-I00), the EU-FP7 “Mediterranean Sea Acidification in a Changing Climate” project (MedSeA; grant agreement 265103), and the Generalitat de Catalunya (MERS, 2021 SGR 00640). J.W.B.R. acknowledges the European Research Council under the European Union’s Horizon 2020 research and innovation program (grant agreement 805246) and B.M. the Severo Ochoa grant CEX2018-000794-S and CSIC LINKA20102. G.L. acknowledges funding from the Spanish Ministry of Universities through a Maria Zambrano grant.

Author contributions

S.P. and P.Z. conceived of the presented idea and organized the outline. S.P., P.Z., R.S., H.V., J.W.B.R., J.G.-O., B.M. developed the methodology. S.P. took the lead in writing the manuscript. S.P. and M.G. provided figures. S.P., P.Z., R.S., H.V., J.W.B.R., E.L., J.G.-O., G.L., M.G. and B.M. contributed to the writing of the article.

Competing interests

The authors declare no competing interests.

Additional information

Supplementary information The online version contains supplementary material available at <https://doi.org/10.1038/s43247-023-00947-7>.

Correspondence and requests for materials should be addressed to Sven Pallacks.

Peer review information *Communications Earth and Environment* thanks Kate Salmon and the other anonymous reviewer for their contribution to the peer review of this work. Primary Handling Editors: Clare Davis. A peer review file is available.

Reprints and permission information is available at <http://www.nature.com/reprints>

Publisher’s note Springer Nature remains neutral with regard to jurisdictional claims in published maps and institutional affiliations.



Open Access This article is licensed under a Creative Commons Attribution 4.0 International License, which permits use, sharing, adaptation, distribution and reproduction in any medium or format, as long as you give appropriate credit to the original author(s) and the source, provide a link to the Creative Commons licence, and indicate if changes were made. The images or other third party material in this article are included in the article’s Creative Commons licence, unless indicated otherwise in a credit line to the material. If material is not included in the article’s Creative Commons licence and your intended use is not permitted by statutory regulation or exceeds the permitted use, you will need to obtain permission directly from the copyright holder. To view a copy of this licence, visit <http://creativecommons.org/licenses/by/4.0/>.

© The Author(s) 2023

© Springer Nature Limited 2023. This work is published under <http://creativecommons.org/licenses/by/4.0/>(the “License”). Notwithstanding the ProQuest Terms and Conditions, you may use this content in accordance with the terms of the License.